รายงานฉบับสมบูรณ์

โครงการ Structural Basis of Oligomerisation and Pore Formation by the *Bacillus thuringiensis* Moquito-Larvicidal Proteins

การศึกษาเชิงโครงสร้างของการรวมตัวและการเกิดรูรั่วโดยโปรตีนฆ่าลูกน้ำยุงจากแบคทีเรีย *Bacillus thuringiensis*

โดย นายชนันท์ อังศุธนสมบัติ

30 เมษายน 2553

สัญญาเลขที่ ***BRG50-8-0003***

รายงานฉบับสมบูรณ์

โครงการ Structural Basis of Oligomerisation and Pore Formation by the *Bacillus thuringiensis* Moquito-Larvicidal Proteins

การศึกษาเชิงโครงสร้างของการรวมตัวและการเกิดรูรั่วโดยโปรตีนฆ่าลูกน้ำยุงจากแบคทีเรีย *Bacillus thuringiensis*

ผู้วิจัย
นายชนันท์ อังศุธนสมบัติ

สังกัด
สถาบันชีววิทยาศาสตร์โมเลกุล
มหาวิทยาลัยมหิดล

สนับสนุนโดยสำนักงานกองทุนสนับสนุนการวิจัย

Acknowledgements

I am grateful to Drs. Wolfgang Fischer, Fred Sigworth, Gerd Katzenmeier, Somphob Leetachewa and Chalermpol Karnchanawarin for valuable comments and helpful discussion and to Somsri Sakdee and Anchalee Nirachanon for technical assistance. This work was supported in part by grant number BRG50-8-0003 from the Thailand Research Fund. Golden Jubilee Ph.D. research scholarships to Puey Ounjai, Kasorn Tiewsiri and Niramon Thamwiriyasati are gratefully acknowledged.

Chanan Angsuthanasombat

April 30, 2010

Project Code: BRG50-8-0003

Project Title:

Structural Basis of Oligomerisation and Pore Formation by the *Bacillus thuringiensis* Moquito-Larvicidal Proteins

การศึกษาเชิงโครงสร้างของการรวมตัวและการเกิดรูรั่วโดยโปรตีนฆ่าลูกน้ำยุงจากแบคทีเรีย *Bacillus thuringiensis*

Investigator: Chanan Angsuthanasombat, Ph.D.

Laboratory of Molecular Biophysics and Structural Biochemistry
Institute of Molecular Biosciences, Mahidol University

E-mail Address: *stcas@mahidol.ac.th*

Project Period: 3 years (May 1, 2007 - April 30, 2010)

Abstract

The insecticidal character of *Bacillus thuringiensis* Cry δ-endotoxins produced is believed to be caused by their capability to generate lytic pores in the target larval midgut membrane. Herein, membrane-associated structures of the 65-kDa mosquito-active Cry4Ba toxin was analysed by electron crystallography. 2D crystals of the oligomeric toxin complex have been captured in two distinct conformations *via* detergent dialysis. Both complexes appeared to be trimeric; one crystal form revealed a symmetrical pinwheel-like shape whilst the other form revealed a propeller-like conformation displaying an obvious hole in the center region, conceivably implying the closed and open states of the pore. We have also characterised the Lipid-induced conformation of a 27-residue Cry4Ba-α7 peptide in different phospholipid membranes. ATR-FTIR results showed that the peptide in DMPC or DDPC adopted both α-helical and β-structure, present in varying proportions depending on the peptide-to- lipid ratio, but only α-helical conformation was observed in anionic DMPG membranes. H^+/D^+ exchange results showed protection of ~90% in DMPC for the β-form, with a peptide carbonyl average tilt angle of ~45^{o} with respect to the bilayer normal, whilst the α-helical form was found preferentially on the membrane surface. 10-ns MD simulations of the α7 peptide in DMPC bilayers supported the stability of α-helical and β-conformations for the membrane-associated and membrane-inserted states, respectively. Moreover, the 65-kDa functional form of the Cry4Ba-R203Q mutant was generated for crystallization by eliminating the tryptic cleavage site at Arg^{203}. The 65-kDa trypsin-resistant fragment has been purified and crystallized using the sitting-drop vapor diffusion method. The crystals belong to the rhombohedral space group *R*32 with unit-cell parameters $a = b = 184.62$ Å, $c = 187.36$ Å. Diffraction data were collected to at least 2.07 Å resolution using synchrotron radiation X-ray and gave a data set with an overall R_{sym} of 9.1% and a completeness of 99.9%. Preliminary analysis indicates that one asymmetric unit contains one molecule of the active full-length mutant with the V_M coefficient and the solvent content of 4.33 $Å^3\ Da^{-1}$ and 71%, respectively.

***Keywords*:** ATR-FTIR, Crystallisation, Electron crystallography, H^+/D^+ exchange, Larvicidal activity, Membrane-associated pore complex, Mutagenesis, Trimeric structure

Introduction

Bacillus thuringiensis (*Bt*), a Gram–positive sporulating soil bacterium, synthesises cytoplasmic crystalline toxin inclusions with larvicidal activity [Schnepf *et al*., 1998]. These cytoplasmic inclusions are composed of one or several insecticidal proteins known as "**δ–endotoxins**" that have been classified as crytalline (Cry) and/or cytolytic (Cyt) toxins based on the similarity of their deduced amino acid sequences [Crickmore *et al*., 1998]. Currently, the Cry toxins have been shown to be toxic to a wide variety of insect larvae in the orders Lepidoptera (moths and butterflies), Diptera (mosquitoes and flies), Coleoptera (beetles and weevils) and Hymenoptera (wasps and bees) [De Maagd *et al*., 2003]. However, the actual underlying mechanism of toxicity remains to be investigated, even the knowledge of how these insecticidal proteins work at the molecular level has increased substantially over the last decade.

Thus far, *Bt* Cry toxin structures have been solved by X–ray crystallography in almost all the major specificity classes, including the lepidoteran–specific Cry1Aa [Grochulski *et al*., 1995] and Cry1Ac [Derbyshire *et al*., 2001], the lepidopteran, dipteran–dual specific Cry2Aa [Morse *et al*., 2001], the coleopteran–specific Cry3Aa [Li *et al*., 1991], and the dipteran–specific Cry4Aa and Cry4Ba [Boonserm *et al*., 2005; 2006]. These three–dimensional structures have provided a greater understanding of the molecular basis of their insect specificity and gut epithelial cell lysis. Although these toxins exert their insecticidal activity against different target insect larvae, they all share a high degree of overall structural similarity and are composed of three structurally distinct domains that are, from the N– to C–terminus, a bundle of α–helices, a three–β–sheet assembly, and a β–sandwich.

The N–terminal domain (**I**) is a group of seven helices in which the most hydrophobic helix 5 is encircled by six other amphipathic helices. Structurally, it is immediately apparent that domain I is likely to be the transmembrane pore–forming apparatus. In addition, it has been experimentally evident that this helical domain is able to form functional pores [Walters *et al*., 1993; Puntheeranurak *et al*., 2004]. A number of studies have demonstrated a crucial role of helices 4 and 5 in pore–forming activity [Gerber & Shai, 2000; Leetachewa *et al*., 2006]. The middle domain (**II**) consists of three anti–parallel β–sheets aligned in β–prism motifs with surface–exposed loops that have been demonstrated to be involved in receptor binding, and hence determines toxin specificity [Pigott & Ellar, 2007]. The C–terminal domain (**III**) is a β–sandwich comprising two anti–parallel β–sheets arranged in a jelly–roll–like topology. The exact role of this domain is still not clearly elucidated, it however has been implicated in receptor recognition [De Maagd *et al*., 2000; Chayaratanasin *et al*., 2007].

Up-to-date, substantial evidence supports an "umbrella–like" model that has been proposed to describe the membrane–bound state of the *Bt* Cry toxins, which involves an

insertion of helices 4 and 5 into the lipid bilayers as a helical hairpin structure, with the remaining helices spreading over the membrane surface [Gazit *et al*., 1998]. A number of mutational studies suggested that helix 4 is aligned to face the pore lumen and participates in ion conduction [Masson *et al*., 1999; Sramala *et al*., 2001], whilst helix 5 interacts with the lipid membrane and is involved in toxin oligomerisation [Nunez—Valdez *et al*., 2001; Likitvivatanavong *et al*., 2006]. Albeit various approaches have been used to enlighten the pore model of the Cry toxins [Loseva *et al*., 2001; Gómez *et al*., 2002; Puntheeranurak *et al*., 2005; Tomimoto *et al*., 2006] and the tetrameric form is widely believed to be the true oligomericity of the Cry toxins, several arguments could still be made.

Experimental Procedures

Construction of a Trypsin-site Elimination Mutant

The pMU388 plasmid encoding the 130-kDa Cry4Ba protoxin under control of the *lac*Z promoter [Angsuthanasombat *et al*., 1987] was used as a template for generating a trypsin-site elimination mutant (R203Q) using a pair of mutagenic oligonucleotides [forward primer, 5′-GGTCTTTAGCAC**AGTCT**GC**A**GGTGACCAACTATATAAC-3′ and reverse primer, 5′-GTTATAG TTGGTCAC**CTGCAGACT**GTGCTAAGACC-3′ (bold letters indicate changed nucleotides and underlined bases indicate a *Pst*I restriction site)]. The trypsin site at Arg^{203} was deleted by substitution with glutamine *via* PCR-based site-directed mutagenesis, following the procedure of the QuickChange Mutagenesis Kit (Stratagene).

Expression & Preparation of Toxin Inclusions

The wild type and mutant toxin genes were expressed in *E. coli* strain JM109 under control of the *lac*Z promoter. Cells were grown in LB medium plus 100 μg/ml of ampicillin until OD_{600} reached 0.4-0.5 and incubation was continued for another 4 hrs after addition of IPTG to a final concentration of 0.1 mM. *E. coli* cultures expressing each mutant as inclusion bodies were harvested by centrifugation, resuspended in 1 ml of distilled water and then disrupted in a French Pressure Cell at 16,000 psi. The crude lysates were centrifuged at 8,000×*g* for 5 min and pellets obtained were washed 3 times in distilled water.

Mosquito-Larvicidal Assays

Bioassays for toxin inclusions were performed using 2-day-old *Aedes aegypti* larvae. The assay was carried out in 1 ml of distilled water containing a serial dilution of toxin inclusions (0.2, 1.0, 2.5, 5, 10, 25 μg/ml) in a 48-well microtiter plate at room temperature (25-30°C), with 10 larvae per well and a total of 100 larvae per toxin concentration. Mortality was recorded after 24-h incubation. LC_{50} values and 95% confidence were calculated using the Probit method of Finney analysis.

Purification & Characterisation of the Activated Toxin

Protoxin inclusions (1 mg/ml) were solubilised in 50 mM Na_2CO_3, pH 9.0 and incubated at 37°C for 60 min as described previously [Angsuthanasombat *et al*., 1991]. After centrifugation for 10 min, the supernatants were analysed by SDS-15% (w/v) PAGE in comparison with the inclusion suspension. Solubilised protoxins (4 mg/ml) were digested with trypsin (*L*-1-tosylamide-2-phenylethyl chloromethyl ketone-treated, Sigma) at enzyme/toxin ratio of 1:20 (w/w) in 50 mM Na_2CO_3, pH 9.0, at 37°C for 16 hrs, and enzyme activity was inhibited by adding phenylmethane sulfonyl fluoride (PMSF) to give a final concentration of 1 mM.

The trypsin-treated fraction was subjected to size-exclusion chromatography (Superdex 200, GE Healthcare) equilibrated with Na_2CO_3 (50 mM, pH 9.0) at a flow rate of 0.4 ml/min. The eluted peak fractions containing the 65-kDa mutant protein were pooled and concentrated to ~10 mg/ml by ultrafiltration using a Centriprep column (30-kDa cutoff, Amicon) before crystallization trials.

Immonoblotting of the purified toxin was performed with the 2F-1H2 MAb which is specific to the Cry4Ba-domain III fragment as previously described [Chayaratanasin *et al.*, 2007]. The homogeneity of the purified 65-kDa activated Cry4Ba toxin was finally evaluated by visualising under negative stained electron microscopy.

Liposome Based-Calcein Release Assays

Large unilamellar vesicles (LUVs) were prepared from 2 mg/ml of a mixture of lipids (Avanti Polar Lipid, USA) of phosphatidylcholine (PC) / phosphatidyl ethanolamine (PE) / cholesterol (Ch) (10:10:1 w/w) dissolved in chloroform. The solvent was evaporated under a N_2 stream and the resulting lipid film was resuspended in 200 µl of 60 mM calcein (pre-dissolved in 100 mM Na_2CO_3, pH 9.0)/10 mM Tris-HCl, pH 9.0. After subjected to 5 cycles of freezing and thawing, the lipid suspension was repeatedly squeezed through a polycarbonate membrane (0.1 µm pore size, Avanti Polar Lipid) for a minimum of 20 passes, using a two-syringe extruder (Avanti Polar Lipid). The untrapped calcein was removed from the LUV suspension by gel filtration on a HiTrap™ desalting column (Amersham Pharmacia Biotech, Uppsala, Sweden). Liposome concentrations were estimated by measuring the lipid phosphorus content, and a final concentration of 1.25 µM LUV was used for the calcein release assay. After adding 5 µl of a sample (5-10 µg) into 400 µl of LUV solution placed in a 1 cm light-path polymethyl methacrylate cuvette (Brand, Germany). The degree of LUV perturbation was determined as increase in the fluorescence intensity of the released calcein. Fluorescence was monitored at 25ºC on a Perkin-Elmer LS50 spectrofluorimeter with excitation and emission wavelengths set at 485 and 520 nm, respectively, and a slit width of 5 nm.

2D Crystallisation of the 65-kDa Activated Toxin

Purified Cry4Ba proteins were diluted to a final concentration of 0.5-1 mg/ml in buffer at a final concentration of 12.5 mM Tris-HCl, 37.5 mM NaCl, 37.5 mM Na_2CO_3 and 10% octylglucoside, pH 8.0 in a total volume of 100 µl. DMPC was added to a final lipid-to-protein mass ratio of 1.0. Highly ordered arrays of membrane associated Cry4Ba toxin were produced by transferring the solution to home-made dialysis buttons (14-kDa cutoff) and dialysing against 50 mM Na_2CO_3 buffer, pH 10.5 for 24-48 hrs at 25°C.

Negative Stain Electron Microscopy & Image Analysis

2D crystals were placed either on air glow discharged (negatively charged surface) or ten days-old desiccated (hydrophobic) carbon coated Cu/Rh grids. Excess sample was removed by blotting with filter paper before staining with three washes of 1% uranylacetate. Samples were analysed using a Technai T12 electron microscope equipped with a LaB6-filament, operated at 120 kV and x 30,000 magnification. Electron microscopic images were recorded with a GATAN 794, 1,024 x 1,024-pixel charge-coupled device camera using a dose of approximately 25 electrons/$Å^2$ at underfocus values that placed the first zero of the contrast transfer function past the resolution cutoff of the reconstructions. Images were corrected for lattice distortion using the MRC software package [Crowther *et al.*, 1996] and projection density maps were calculated in CCP4.

Peptide Preparation & Purification

A 27-residue synthetic peptide corresponding to α7 of the Cry4Ba toxin was purchased from W.M. KECK Foundation Biotechnology Resource Laboratory, Yale University. Isotopic

labeling of helix 7 with C^{13}=O^{18} at Val^{18} and nitrile-derivatised (C≡N) side-chain at Phe^{7} (corresponding to the positions Val^{257} and Phe^{246}, respectively) were performed as internal local environment markers. Purification of the α7 peptide was accomplished by a reverse-phase high-performance liquid chromatography (RP-HPLC) system using a Jupiter C_{18} column (3 μm particle size, 120-Å pore size, 4×50 mm, Phenomenex, USA). Chromatographic separation was achieved with a linear gradient of B in A (A = 0.05% TFA in H_2O; B = 0.05% TFA / 20% H_2O / 80% acetonitrile). Liquid chromatography-mass spectrometry (LC-ESI-MS) was employed to verify the purity of the α7 peptide.

The purified peptide (300 μg, lyophilised powder) was resuspended in each lipid solution (DMPC, DDPC and DMPG in hexafluoroisopropanol), resulting in a peptide-lipid ratio of 1:5, 1:30 and 1:100 (mol/mol). Each mixture was swirled gently and applied onto a trapezoidal germanium (Ge) internal reflection element of 50 mm × 2 mm × 20 mm (Graseby Specac, Kent, UK). Adsorbed water vapour from a humid atmosphere was removed using a dry N_2 stream. For hydration under D_2O and H^+/D^+ exchange experiments, spectra were collected after flushing the interior of the sample cell with D_2O-saturated N_2, obtained by bubbling dry N_2 through two compartments containing D_2O for 1 h.

ATR-FTIR Measurements

IR spectra were collected from a Nicolet Nexus 470 spectrometer purged with N_2 and equipped with a MCT/A detector cooled with liquid N_2. Typically, interferograms were recorded with 4 cm^{-1} spectral resolution with a 25-reflection ATR accessory (Graseby Specac) and a wire grid polariser (0.25 μm, Graseby Specac), A total 200 interferograms were averaged for one spectrum using 1-point zero filling and Happ-Genzel apodisation using either parallel (0°) or perpendicular (90°) polarised light.

Spectra were collected either after removal of bulk water or after hydration with D_2O as described previously [Marsh, 1999]. Briefly, in the first case, the dichroic ratio (R^{ATR}) of the amide I band (C=O stretching) and the band at 2850 cm^{-1}, derived from the CH_2 stretching of the lipid, was recorded. In the second case, after hydration with D_2O, R^{ATR} of the amide A band (N-H stretching) was also recorded. Dichroic ratios were calculated as the ratio between the integrated absorptions collected from parallel and perpendicular polarised light.

ATR-FTIR Data Analysis

Secondary structure of a peptide in the lipid membrane environment was determined using the corrected ATR spectra which were obtained from the parallel (∥) and perpendicularly (⊥) polarised spectra, according to 1 (∥) + 1.44 (⊥) as described previously [Marsh, 1999]. The amide I band was Fourier self-deconvolved (FSD) with a full-width at a half-height of 20 cm^{-1} and an enhancement factor *k* of 2.0. Peak integration for the amide I was performed on these FSD spectra from 1700 to 1600 cm^{-1}. For the amide A band and the band at 2850 cm^{-1}, integration was performed without FSD from 3400 to 3200 cm^{-1} and from 2890 to 2800 cm^{-1}, respectively.

Helix tilt (β) was calculated from the order parameters (S) for the helix S_{helix} and the lipid S_{lipid} [Chia *et al*., 2002] according to the following formula:

$$S = \frac{\varepsilon_X^2 - R^{ATR}\varepsilon_y^2 + \varepsilon_z^2}{\varepsilon_X^2 - R^{ATR}\varepsilon_y^2 - 2\varepsilon_z^2} \div \frac{3\cos^2\alpha - 1}{2} \qquad (Eq.\ 1)$$

$$S_{helix}' = \frac{S_{helix}}{S_{lipid}} \qquad (Eq.\ 2)$$

$$S_{helix}' = \frac{3(\cos^2\beta) - 1}{2} \qquad (Eq.\ 3)$$

R^{ATR} is the dichroic ratio of amide I or amide A (for S_{helix}) and the dichroic ratio of the 2850 cm^{-1} band (for S_{lipid}). The angle α is 90° for the lipid symmetric CH_2 stretching, 39° for the peptidic C=O bond and 29° for the N-H bond [Chia *et al*., 2002]. The tilt angle of the β-strands relative to the membrane normal (*z* axis) was determined by using α=90° for the C=O bond within the β-sheet environment [Tamm & Tatulian, 1997]. The parameters (electric field components of the evanescent wave) ε_x = 1.398, ε_y = 1.516 and ε_z = 1.625 are the integrated absorption coefficients for a Ge reflection element. Since the thickness of the final film sample was roughly estimated to be more than 10 μm, while the amplitude of the evanescent wave decays (at $1/\varepsilon$ at its initial value) after 1 μm in a Ge plate, the values for these components are those given by [Harrick, 1967] according to a thick-film approximation. The contribution of S_{lipid} to S_{helix} was taken into account and the β was calculated from S_{helix}'. H^+/D^+ exchange was calculated from the ratio of amide II to amide I, before and after the exchange using the corrected ATR spectra that were obtained as mentioned earlier.

Peptide/Bilayer/Water Simulating System & MD Simulations

Helical and β-structure models of the 27-residue α7 peptide were generated by using a combined simulated annealing and MD simulations (SD/MD) approach *via* Xplor [Brünger, 1992] and What if programs [Vriend, 1990]. The conformation of the α-helical model was obtained from the Cry4Ba atomic coordinates [Boonserm *et al.*, 2005]. For the β-conformation, it was predicted to be a β-hairpin based on the Chou-Fasman method [Chou & Fasman, 1978] and the most stable configuration was selected after equilibrating in the lipid environment for 1 ns.

For the helical form lying at the lipid-water interface, the system contains 243 DMPC (initial set-up 288 DMPC molecules) and 12199 water molecules (the SPC model) with a Na^+ ion added at the position corresponding to the lowest Coulomb energy of the ion. In peptide-orientation setup details, the helical model was oriented perpendicular to the bilayer normal, with its Phe_{CN}^7 side-chain pointing towards to the hydrophobic core of the lipid membrane according to ATR-FTIR experiments. On the other hand, the β-hairpin model was embedded transversely in a pre-equilibrated lipid bilayer (128 DMPC solvated in 6108 SPC water molecules) such that its long axis was parallel to the bilayer nornal. Unfavorable lipid-protein contact made necessary the removal of 32 DMPC molecules, giving a final total of 96 lipid molecules. Each system was minimised and equilibrated for 400 ps prior to unrestrainted MD simulations.

MD simulations were performed using the program package GROMACS 3.2.1 software (http://www.gromacs.org), employing an NPT ensemble (*i.e.*, constant number of particles, pressure and temperature) with a time-step simulation of 2 fs. The simulated pressure was 1 bar, and the temperature was 300 K. Anisotropic pressure-coupling [Berendsen *et al.*, 1984] in *x*-, *y*- and *z*-directions was employed so that the area per lipid was allowed to be adjusted during the simulations. The Berendsen temperature-coupling was carried out with a coupling constant of 0.1 ps. LINCS algorithm [Hess *et al.*, 1997] were used to keep all bond lengths constrained. Long-range electrostatic interactions were calculated using the particle-mesh Ewald method [Essmann *et al.*,1995]. Lennard-Jones and short-range Coulombic interactions were cut off at 1.0 nm.

Protein Crystallization

Crystals were grown by vapor-diffusion method in sitting drops. 0.5 μl of the purified protein (~10 mg/ml) was mixed with an equal volume of the reservoir solution containing ammonium acetate (0.05 M), $MgCl_2$ (0.01 M), (+/-)-2-methyl-2,4-pentanediol (MPD, 5-10%, *v/v*) in Tris-HCl buffer (0.05 M, pH 7.0-8.0) (modified from the screen kit Natrix #43, Hampton Research). The mixture drop was then equilibrated against 100 μl of the reservoir solution at 20°C. Crystals appeared after a period of 15 days to four weeks and grew to their maximum size in three months.

The dissolved Cry4Ba-R203Q crystals were subjected to SDS-PAGE (12% gel), and subsequently eluted out from the excised gel and digested with trypsin according to the standard protocol. Trypsin-generated peptide fragments were separated on a C18 column (0.18×100 mm, Thermo Electron, USA) and analyzed by liquid chromatography-tandem mass spectrometry (Finnigan LTQ Linear Ion Trap Mass Spectrometer) as performed by Genome Institute, BIOTEC, Thailand.

Crystallographic Data Collection & Processing

The crystal was transferred from a crystallization drop into a cryo-protectant solution (5 µl) containing ammonium acetate (0.05 M), $MgCl_2$ (0.01 M), MPD (10%, (*v/v*)) and glycerol (20 %, (*v/v*)) in Tris buffer (0.05 M, pH 7.5) for a few seconds and mounted on a synthetic nylon loop (0.1 - 0.2 mm, Hampton Research Co.), and then flash-cooled in liquid nitrogen. X-ray diffraction data were collected at the beam line BL13B1 equipped with CCD detectors (Q315, ADSC) at the National Synchrotron Radiation Research Center (Hsinchu, Taiwan). For complete data collection, 90° rotations with 1.0° oscillation were measured using X-ray wavelength of 1.00 Å, exposure duration 10 s and a distance 300 mm from the crystal to the detector, at 110 K in a nitrogen stream using a cryo-system (X-Stream, Rigaku/MSC, Inc.). All data were indexed, integrated and scaled using the program *HKL2000* [Otwinowski & Minor, 1997].

Results & Discussion

Membrane-associated Cry4Ba Complex via Electron Crystallography

Up until now, the number of subunits of the *Bt* Cry toxins that constitute a functional pore complex or whether the oligomarisation occurs in the membrane-bound state has been still under debate (*see* **Table I**). In this report, we have therefore employed electron crystallography to gain more critical insights into the lipid-associated structure and oligomeric state of the Cry4Ba mosquito-larvicidal protein.

Cry4Ba protoxin was expressed in *E. coli* as inclusion bodies, isolated from cell lysate, and digested with trypsin. Size-exclusion chromatography of the protein preparation (**Fig. 1A**) showed two toxin-related peaks. Peak 1, which was eluted with the void volume, contained aggregates of protein; under negative stain, electron microscopy shows some structures resembling a three-bladed propeller (**Fig. 1A1**). Peak 2 contained toxin monomers as judged from the size of particles (about 60 Å) seen in electron micrographs (**Fig. 1A2**). Peak 2 was used for further characterisation. The two peaks represent inter-convertible species, as a second chromatographic separation of either the peak 1 or peak 2 fraction yielded the same two peaks.

A protein gel of peak 2 (**Fig. 1B**) shows prominent bands at ~49 and ~19 kDa, corresponding to the active toxin fragments resulting from a cleavage site in the loop connecting α5 and α6 [Angsuthanasombat *et al.*, 2004]. The exact mass of the purified protein was measured by mass spectrometry. The molecular weights were 18856.4±0.6 and 49687.3±3.6, respectively. The protein gel also shows a 200-kDa band. Western blotting with a monoclonal antibody to Cry4Ba-domain III also labels this 200-kDa band, supporting the idea that it may

arise from a toxin trimer. Western blotting of the peak 1 fraction shows a similar pattern of protein bands, except that the 200-kDa trimer band was more prominent. We conclude that the Cry4Ba protein exists as an unstable trimeric intermediate about 200 kDa in size. To verify the functional integrity of the purified Cry4Ba protein, toxin-induced release of the fluorescent dye calcein from liposomes was measured as a function of Cry4Ba toxin concentration. Purified toxins were able to induce efflux of the calcein from receptor-free liposomes with a maximal activity of about 60% (**Fig. 1C**), similar to the degree of release seen in other preparations of functional toxin.

To determine the structure and oligomeric state of the Cry4Ba toxin-induced pore in the lipid bilayers, we have crystallised the 65-kDa purified toxins in the presence of DMPC lipid by detergent dialysis technique. In this study, the crystals obtained were allowed to adsorb on both hydrophobic and negatively charged carbon surfaces. When images of suitable crystals were collected at a nominal magnification under low-dose conditions used here, well ordered 2D crystal patches of the average size around 1x1 μm were distinctly observed on both grids. It should be noted that some lipid vesicles were also detected on the glow discharged grid; but on the hydrophobic grids, we found some lipid plates coexisted with the crystals. Both crystals were able to be diffracted upto 15 Å (**Fig. 2A, 2B**), indicating that the protein is actually very well preserved in the negative stain. Unexpectedly, despite the fact that the calculated projection maps of 2D crystals from both grids reveal p3 symmetry, representing a similar trimeric structure, slight disagreement in unit cell dimension was exclusively observed. The cell of hydrophobic-bound 2D crystal is $a = b = 112$ Å, $\gamma = 120°$ and the charge-bound crystal has unit cell dimensions of $a = b = 107$ Å, $\gamma = 120°$. Moreover, the calculated projection structures clearly displayed different conformation of the three-domain Cry4Ba protein. The propeller-like structure was obtained from the charged surface while the hydrophobic-bound trimeric structure has a pinwheel-like appearance, demonstrating that this 65-kDa three-domain toxin had undergone some significant rearrangement (**Fig. 3**).

Resembling other ion channels, the Cry toxin-induced pores or channels would possibly undergo a conformational change upon gating of the protein. Even if at this stage the gating mechanism of the pore-forming Cry toxins is still unrevealed, several planar lipid bilayer experiments strongly suggested that the channels induced by Cry toxins exhibit at least two different functional states: closed and open [Masson *et al*., 2002; Puntheeranurak *et al*., 2004]. Could these two trimeric conformations observed here be the closed and open states of the Cry4Ba toxin? Indeed, they could likely be each functional state since some major structural differences were seen at the pore mouth and peripheral region for both trimers (*see* **Fig. 3**).

It is worth mentioning that the pinwheel-like structure exhibited a very clear clockwise handedness in that the L-shape blades which could represent the domains II and III of the

three-domain Cry4Ba toxin pointing towards the same direction, whilst the central region which is likely to embody the pore-forming domain I is relatively small (**Fig. 3B, 3D**). Surprisingly, the projection map of this pinwheel structure showed virtually no depression in this region even when the map was calculated at 17 Å resolution (**Fig. 3D**). Notwithstanding the lack of detailed functional characterization, this pinwheel-like structure might perhaps represent the closed state of the Cry4Ba toxin-induced pore in the membrane.

Then again, the central region of the propeller-like conformation is significantly larger with the stain excluded region in the center of the map (**Fig 3A, 3C**), which could possibly reflect a cavity of an open pore. This pore configuration can actually be seen even when the map was calculated at 20 Å resolution (**Fig. 3A**), suggesting that the pore if present must be larger than 20 Å. This result is in good agreement with the estimated pore size from permeation experiments for Cry1Ab [Soberón *et al.*, 2000] and the blockade of various sizes of polyethylene glycols for Cry1Ca [Peyronnet *et al.*, 2002] in that the pore size should be in the range of 10-26 Å. Actuality, the plane group symmetry of this crystal form can be either p3 or p312 as defined by ALLSPACE [Unger *et al.*, 1997]. Nonetheless, we believe that the additional two-fold axis parallel to the membrane plane of the propeller blade was unlikely to be the real feature of the protein otherwise all the molecules would have to have exactly the same orientation when they bind to the membrane. Therefore, from our view, this propeller-like structure is more likely to belong to the p3 plane group similar to the other form of crystal. In addition, a major conformational change observed in the blade region of the trimer leads us to an assumption that the toxin molecules are associated peripherally with the lipid membrane and would insert only small part of the protein, *i.e.* the α4-loop-α5 transmembrane hairpin, into the lipid layers as proposed earlier [Gazit *et al.*, 1998].

As mentioned earlier, the projection map of the propeller-like structure appears to have a pore in the middle even at 20 Å resolution (*see* **Fig. 3A, 3C**), which could possibly reflect the cavity of the open-state Cry4Ba complex. This feature is absence in the pinwheel-like structure (*see* **Fig. 3B, 3D**). Since almost all ion channels have been found to be gated by different stimuli including pH [Vinothkumar *et al.*, 2005], ligands [Jiang *et al.*, 2002] and voltages [Sigworth, 1994]. In this manner, one important caveat here that could apply to the results observed for the propeller feature is that the surface charge on the grid would possibly generate enough voltages to trigger the pore opening. This could nonetheless also happen due to the fact that the different forms of crystals bind preferentially to the certain surfaces. Thus, this notion remains to be verified by performing further more structural and electrophysiological experiments.

In conclusion, the two symmetrical trimeric conformations of the membrane-associated Cry4Ba toxin complex were observed in the 2D crystals on the different charge surfaces.

Although the crystallographic resolution was still insufficient to give such critical insights into the structural details of the toxin-induced pore architecture, we have here provided pivotal evidence for the first time that the 65-kDa activated Cry4Ba toxin could have at least two conformational states in association with the lipid membrane, implying the closed and open states of the pore. Further investigation for more details of the toxin-induced pore complex within the lipid membranes is of great interest.

Lipid-induced Conformation of α7 from Cry4Ba Toxin

In our earlier studies, we have made a single-proline substitution in α7 of the Cry4Ba toxin, and found that the integrity of α7 conceivably plays a role in toxicity [Sramala *et al.*, 2000]. Additionally, we have strengthened the functional significance of α7 by showing that the highly conserved aromaticity of Tyr^{249} and Phe^{264} within this helix plays an important role in larvicidal activity of the Cry4Ba toxin [Tiewsiri & Angsuthanasombat, 2007]. To gain a more critical insight into the role of this conserved helix in toxicity mechanism, a 27-residue synthetic peptide corresponding to the Cry4Ba-α7 (*see* **Fig. 4**) was structurally and functionally characterised with respect to its interaction with the lipid membrane.

ATR-FTIR spectroscopy was employed to determine the peptide structure of Cry4Ba-α7 when reconstituted in three different types of phospholipid multibilayers, *i.e.* zwitterionic (DMPC and DDPC) and negatively charged (DMPG) phospholipids. As shown in **Fig. 5**, the frequencies of the amide I region of the α7 peptide after mixing with DMPC at peptide-to-lipid molar ratio (P/L) of 1:5 showed two major absorption peaks at 1654 and 1633 cm^{-1} that are assigned to α-helical and β-sheet structures, respectively. This indicates that the 27-residue α7 peptide could adopt both α-helical and β-conformations in a DMPC membrane-bound state. However, only one major amide I absorption peak of the peptide was found centered at 1655 and 1631 cm^{-1} when mixed with DMPG and DDPC, respectively, indicating that the peptide reconstituted in DMPG is mainly α-helical, whilst the peptide within DDPC adopts predominantly a β-structure. Thus, conformation of the Cry4Ba-α7 peptide is essentially influenced by the lipid composition.

We also conducted experiments to explore an effect of the change in P/L on the peptide structure of Cry4Ba-α7. **Table 2** lists the relative distribution of the secondary structure elements for the α7 peptide observed in various conditions. For DMPC at P/L of 1:100, the portion of the α-helical structure was enhanced (~90%) when compared to P/L of 1:30 (~65%) and of 1:5 (~50%) while the β-structure decreased in the same direction. A similar behavior was also found when the peptide was mixed with DDPC membranes (*see* **Table 2**). However, the peptide adopts only α-helical conformation when reconstituted in the anionic DMPG membrane for all three P/L ratios. The peptide was α-helical for all three types of lipids at P/L

of 1:100, indicating that this peptide is rather stable in an α-helical conformation at a high lipid concentration, independently from the lipid environments.

Further quantitative analysis was performed to determine the orientation and membrane insertion of the Cry4B-α7 peptide when reconstituted in DMPC, DMPG and DDPC membranes. As described earlier with ATR-FTIR, the percentage of membrane-inserted residues can be determined by measuring the amide I/amide II ratio before and after hydration with D_2O [Marsh, 1999] and the orientation of the peptide can be obtained from the dichroic ratios of amide I or amide A bands [Arkin *et al*., 1996]. The amide II absorption band (1544 cm^{-1}) for the α7 peptide in DMPC membranes was still present after 1-h exposure to D_2O (**Fig. 6A**, *arrow*), indicating that part of the peptide molecule is protected from the D_2O exchange and embedded in the lipid membrane. Moreover, examination of the ratio between non-polarised amide II and amide I before and after D_2O exchange revealed that ~90% of the β-form peptide was inserted in the DMPC membrane, whilst only ~40% of the α-helical form did not exchange in D_2O. In similar experiments using DMPG or DDPC membranes, the percentage of non-exchanged amide groups was ~95% for the α-helical form in DMPG (**Fig. 6B**), and ~91% and ~50% for the β- and helical conformations, respectively, in DDPC (**Fig. 6C**).

The orientation of the α7 peptide with respect to the lipid membrane was obtained from the dichroic ratios of amide I or amide A bands (see **Table 3**). It is noteworthy that the dichroic ratio of the band at 2850 cm^{-1} from the methylene CH_2 stretching of DMPC, DMPG and DDPC reconstituted with the peptide was found to be 1.1, 1.2 and 1.1, respectively, indicating that all the phospholipid membranes used under experimental conditions are typically well-ordered bilayers [Marsh, 1999]. For the β-form peptide in DMPC, after hydration in D_2O, the dichroism of the amide I ($R_{AI\beta}$ = 1.8) indicated that the carbonyl bonds of the peptide were oriented with an average tilt of ~41° or ~48° (R_{AA} = 1.6), whilst that of the α-helical form ($R_{AI\alpha}$ = 1.8) suggested that the non-exchange part of this conformation was not inserted in, but rather lying mostly parallel to, the membrane surface. The helix tilt of the helical form in the anionic phospholipid (DMPG) was ~43° to the membrane normal, with the amide A dichroic ratio (R_{AA}) of 2.0. In addition, when the shorter-acylchain phospholipid (DDPC) was employed, the amide I band dichroism of the α7 peptide indicated that the α-helix was most likely on the membrane surface ($R_{AI\alpha}$ = 1.1), whereas the β-conformation which penetrated into lipid membrane was oriented with a tilt angle of ~18° ($R_{AI\beta}$ = 1.2). The tilt angle in the latter case (β-form in DDPC) was also calculated with the more reliable amide A dichroism (R_{AA} = 1.6), giving a tilt angle of ~40°.

At this stage, our ATR-FTIR studies reveal that both structural conformation and insertion behaviors of the Cry4Ba-α7 peptide in either DMPC or DDPC are rather similar, exhibiting a helical conformation laying on the membrane surface and a β-structure penetrating into the lipid membrane. Thus, this lipid-induced β-conformation observed in only zwitterionic DMPC and

DDPC membranes, which are more relevant to the target cell membranes than DMPG, might have a functional role in toxicity.

MD simulations of the α7 peptide in an explicit DMPC bilayer were carried out to study the structural conformations and dynamics of the peptide in both α-helical and β-structure conformations. Unlike the α-helical conformation which is taken from the Cry4Ba crystallographic structure [Boonserm *et al.*, 2005], the β-conformation which is assumed to be a β-hairpin was derived from the most stable configuration. In accord with the ATR-FTIR data, the α-helical form was oriented parallel to the membrane water-interface with the Phe_{CN}^{7} side-chain facing the hydrophobic milieu of the membrane, whilst the β-hairpin model was inserted transversely into the membrane with its long axis parallel to the bilayer normal.

Fig. 7 shows the results of MD simulation trajectories for a fully hydrated DMPC-α7 system. An overall measure of the structural stability of the DMPC-associated α7 peptide in each model system was obtained by comparing the time-dependent C_α atoms of root mean square deviations (RMSD) from its starting structure (**Fig. 7A**). For the α-helical model simulations, there is a small overall change in the backbone conformation, with RMSD of 0.18 ± 0.04 nm over the period of 10 ns. This rather differs from the β-hairpin model simulations, in which the large overall change in the C_α RMSD is from 0.27 ± 0.03 nm (average for t < 2 ns) to 0.35 ± 0.05 nm (average for t = 2 to 10 ns). This large deviation is likely due to the arrangement of the amino acid side-chains so that the polar and charged residues would compensate the unfavourable side-chains in the low dielectric core of the lipid bilayer. In addition, analysis of the time evolution of secondary structures reveals that α-helicity of this DMPC-associated helical conformation is largely preserved throughout the 10-ns simulations (**Fig. 7B**). Likewise, in the β-hairpin model simulations, the initial β-conformation is retained primarily in residues 7-13 and 20-27 throughout the period of simulations (**Fig. 7C**).

To visualise the structural change and orientation of each conformation of the DMPC-associated α7 peptide, snapshots of MD simulation trajectories are shown in **Fig. 8**. The 10-ns MD trajectories for the α-helical conformation clearly reveal that this helical peptide is still located at the lipid-water interface, tilted with respect to the horizontal membrane plane by ~90° (**Fig. 8B**). In the simulations starting with the β-hairpin conformation inserted into the bilayer, it still remained in an inserted orientation with a tilt angle of ~40° (**Fig. 8D**). Thus, the MD simulation data support the ATR-FTIR results in as much the α-helical form of the α7 peptide remains intact in a surface-associated orientation. The membrane-inserted orientation is also stable for the β-conformation. Thus,

Other studies with the bacterial toxin pneumolysin have shown that there is a conformational transition from the membrane-bound pre-pore to the transmembrane pore by the

substantial refolding of α-helical regions into membrane-inserted β-hairpins [Tilley *et al.*, 2005]. It has been shown that the hydrophobic stretch (PLVG) at the apex of transmenbrane β-hairpin plays a crucial role in driving the membrane insertion of the aerolysin pore-forming toxin [Iacovache *et al.*, 2006]. This may conceivably reflect our results that α-helix 7 in the Cry4Ba pore-forming domain might be able to refold into an extended β-hairpin with the hydrophobic turn (M-I-VL, *see* **Fig 8D**, *inset*) to insert into the membrane, albeit the hairpin containing several charged and polar-uncharged residues that are energetically unfavourable for membrane insertion. We thus propose that this β-conformation induced by an interaction with zwitterionic membranes would possibly impart greater ability to the toxin molecule to protrude the transmembrane helical hairpin, *i.e.* α4-loop-α5, from the bundle to act as an initiator of membrane penetration.

To further validate the potential effect of the α7 peptide on the integrity of lipid membranes, entrapped dye-release experiments were carried out to access peptide-induced perturbation of liposomes. Herein, LUVs of PC/PE/Ch compositions, which are more biologically relevant to the insect cell membranes, were created with self-quenched fluorescence dye, *i.e.* calcein, entrapped in their interior cavity. The release of the entrapped calcein from LUVs was measured as the 'dequenching' of the calcein fluorescence, and was thereby monitored continuously as an increase in the fluorescence intensity. Under the conditions used in the assays, the α7 peptide (~2 μM) was able to perturb the lipid packing and cause leakage of the encapsulated calcein (**Fig. 9**). As can be inferred from the ATR-FTIR and MD simulations studies, the α7-induced disruption of PC/PE/Ch vesicles could possibly be caused by either a membrane-associated α-helical form or a membrane-inserted β-hairpin. Electrostatic interactions between the phospholipid headgroups and the charges within the α-helical form lining on the membrane surface as well as the membrane penetration of the β-hairpin conformation could lead to some extent of perturbation of the membrane integrity, causing leakage of vesicular contents.

In conclusion, our ATR-FTIR studies have provided pivotal evidence that the Cry4Ba-α7 peptide when reconstituted into zwitterionic phospholipids could adopt either an α-helical conformation that prefers a membrane surface location or a β-structure with a membrane-inserted orientation. Conceivably, the lipid-induced β-conformation of α7 might serve as a lipid anchor needed for an efficient insertion of the pore-forming Cry toxin into the bilayer membrane. However, it remains a challenge for experimental approaches to provide more structural and functional details of such a lipid-induced β-structure. Further simulations exploring the possibility of dynamic refolding of this helix between a membrane-associated α-helical form and a membrane-inserted β-hairpin are also of great interest since this would shed light on toxicity mechanism of the Cry insecticidal proteins.

Crystallization & Preliminary X-ray Analysis of Full-length Cry4Ba

As memtioned earlier, the Cry4Ba protoxin is proteolytically activated *in vitro* by trypsin to two protease-resistant fragments of ~47 and ~20 kDa that remain non-covalently associated, forming a 65-kDa active toxin [Angsuthanasombat *et al*., 2004]. These two trypsin-fragments were produced by cleavage at Arg^{203} which is located in the exposed loop connecting α5 and α6 within the pore-forming domain [Angsuthanasombat *et al*., 2004]. Previously, an incomplete structure of the 65-kDa chymotrypsin-treated Cry4Ba toxin has been reported, with the absence of N-terminal helices due to proteolysis [Boonserm *et al*., 2005]. It is possible that chymotrypsin treatment produced heterogeneous protein fragments by cleavage at alternative N-terminal sites of the Cry4Ba native toxin. Thus glutamine substitution of Arg^{203} of Cry4Ba resulting in resistance to further proteolytic digestion should be of great use in determining the full-length three-dimensional structure. In this study, we have therefore generated a Cry4Ba-R203Q mutant of full length that retains its biologically activity. The purification and crystallization together with preliminary X-ray crystallographic analysis of the 65-kDa trypsin-activated mutant protein are also carried out.

Upon IPTG induction, the 130-kDa Cry4Ba-R203Q mutant protoxin was predominantly produced as a crystalline inclusion which was partially purified from *E. coli* lysate and solubilized in carbonate buffer (pH 9.0), giving a solubility greater than 70% comparable to the wild-type inclusion under similar conditions. After activation by trypsin, the activated mutant toxin was successfully purified by gel filtration as a single peak at the elution volume corresponding to a 65-kDa monomer which was obtained with a purity greater than 90% as analyzed by SDS-PAGE (*see* **Fig. 10**).

For assessment of mutational effect on toxicity, Cry4Ba-R203Q mutant toxin inclusion was tested for its relative biological activity against *A. aegypti* mosquito larvae. The result shown in **Table 4** revealed that the mutant toxin still retains a high larvicidal activity comparable to the wild-type toxin. This indicated that the elimination of the tryptic cleavage site at Arg^{203} by glutamine substitution (R203Q) had no detrimental effect on the Cry4Ba toxicity.

In analogy to our previous study of Cry4Aa [Boonserm *et al*., 2004], we successfully crystallized the 65-kDa trypsin-activated Cry4Ba-R203Q protein. The well formed crystals were obtained when using 0.05 M ammonium acetate, 0.01 M $MgCl_2$ and 10% (*v/v*) MPD in 0.05 M Tris-HCl, pH 7.5 (**Fig. 11**). It is noteworthy that when the dissolved crystals were verified by LC/MS/MS to confirm the presence of intact 65-kDa Cry4Ba-R203Q protein, all parts of trypsin-generated peptide sequences were found to perfectly match the corresponding Cry4Ba mutant sequence (residues Lys^{57}-Ile^{633}). This indicated that the crystals of the activated Cry4Ba-R203 toxin still retain the complete molecule containing the N-terminal fragment, which differs from those of the 65-kDa chymotrypsin-treated native toxin lacking the N-terminal α1–α2b helices [Boonserm *et al*., 2005].

Analysis of the X-ray diffraction data (**Fig. 12**) indicated that the crystals belonged to the rhombohedral space group *R*32, with unit-cell parameters $a = b = 184.62$ Å, $c = 187.36$ Å. The complete data set was collected to a resolution of 2.07 Å consisting of 74,138 unique reflections with an R_{sym} of 9.1%. Assuming one activated toxin molecule (molecular weight of ~65,000) per asymmetric unit, the Matthews coefficient (V_M) of the crystal [Matthews, 1968] was calculated to be 4.33 $Å^3$ Da^{-1}, giving the estimated solvent content of 71%. The data statistics are summarized in **Table 5**.

A preliminary model of Cry4Ba-R203Q structure was solved by molecular replacement. A cross-rotation function search [Tong & Rossmann, 1997] was calculated to determine the correct rotational orientation of the search model in the cell of the unknown structure. Using the truncated Cry4Ba coordinates (PDB code 1W99) [Boomserm *et al*., 2005] as a search model with data from 30.0 to 4.0 Å resolution, the obtained correct solution indicated the high homology between the mutant and template models, suitable for phasing by molecular replacement. Using this orientation matrix, a translation function search [Brunger *et al*., 1990] gave a unique solution with a correlation coefficient of 0.62. The packing value is also high, indicating minimal overlap of the molecule with itself. Following translation function search, rigid body refinement was used to fix and optimize the orientation and translation position of the poly-alanine search model and gave an initial R_{work} of 27.7% for data from 30.0 to 2.0 Å resolution. For improving the model, the optimized position of one molecule per asymmetric unit was subjected to molecular dynamic refinement using *CNS*. The simulated annealing was initially applied globally for the whole molecule, individual domains, and then only to main chain atoms within the resolution range 30.0 to 2.0 Å, giving R_{work} of 26.0%. Using torsion angle dynamics, the number of parameters hence reduces the degree of overfitting of the data. After each round of refinement, the model was inspected with $2F_o$-F_c and F_o-F_c maps to reduce the noise in the electron density maps. The initial calculated electron density maps generated with the phases from the partial model (516 residues) were of excellent quality, the main-chain electron density was continuous, and side-chain electron density was in agreement with the sequence of the Cry4Ba mutant. Further manual model building and refinement aimed at defining the complete Cry4Ba-R203Q structure are in progress.

Table 1: Proposed oligomeric membrane-bound state of a 65-kDa active form of *Bt* Cry toxins

Oligomericity	Toxin	Oligomer size	Experimental approach
Dimer	Cry1Ab Cry1Ac	~130 kDa	Western blotting of BBMV[1]-treated toxins after analysis by modified SDS-PAGE [Tigue *et al.*, 2001].
Trimer	Cry1Aa, Cry1Ab Cry1Ac	~200 kDa	Western blotting of BBMV[1]-treated toxins after analysis by modified SDS-PAGE [Aronson *et al.*, 1999; Kumar & Aronson, 1999].
Trimer	Cry1Ab	Diameter ~10 nm	Electron crystallography of 2D crystals of lipid-bound toxins [Muñóz-Garay *et al.*, 2009].
Trimer	Cry4Ba	~200 kDa	Western blotting of liposome-treated toxins after analysis by modified SDS-PAGE [Likitvivatanavong *et al.*, 2006].
Tetramer	Cry1Aa	Diameter ~5 nm	AFM[2] of toxins inserted in bilayers in liquid cell [Vie *et al.*, 2001].
Tetramer	Cry1Ab	~250 kDa	SDS-PAGE of ScFV73[3] cross-linked toxins [Gómez *et al.*, 2002].
Tetramer	Cry4Ba	Diameter 20-30 nm	AFM[2] of toxin inserted in bilayers in liquid cell [Puntheeranurak *et al.*, 2005].
Multimer	Cry11Aa	~250 kDa	Western blotting of BBMV-associated toxins after analysis by modified SDS-PAGE [Fernandez *et al.*, 2009].

[1]BBMVs = Brush-border membrane vesicles prepared from susceptible insect larval midguts

[2]AFM = Atomic force microscopy

[3]ScFV73 = A single chain antibody mimicking Bt-R1 receptor

Table 2: Estimated percentage of secondary structure contents of the Cry4Ba-α7 peptide in DMPC, DMPG and DDPC with different peptide-to-lipid ratios

Sample (peptide-to-lipid)	Secondary structure (%)[a]					
	DMPC		DMPG		DDPC	
	α-helix	β-sheet	α-helix	β-sheet	α-helix	β-sheet
Helix 7 (1:5)	50	50	100	-	23	77
Helix 7 (1:30)	65	35	100	-	43	57
Helix 7 (1:100)	90	10	100	-	87	12

[a] Standard deviation of each value is < 5%.

Table 3: Orientation analysis of the Cry4Ba-α7 peptide in DMPC, DMPG and DDPC at peptide-to-lipid molar ratio of 1:30

Lipid system	Bulk water removed (H_2O)		Hydrated membrane (D_2O)					
	R_{AI}	R_{AA}	R_{AI}	R_{AA}	R_{ISO}	Exchanged (%)		β°
						α	$\beta_{hairpin}$	
DMPC	1.5±0.2	1.8±0.1	1.8±0.01	1.6±0.1	1.8±0.1	60±7.1	10±4.2	65°±2.6
DMPG	3.7±0.1	2.0±0.2	2.6±0.1	2.0±0.2	3.2±0.06	4±3.2	-	37°±4.9
DDPC	1.7±0.1	1.5±0.1	1.1±0.05	1.6±0.05	1.2±0.04	52±6.4	9±6.4	53°±4.9

Dichroic ratios of amide I (R_{AI}), of amide A (R_{AA}) and of isotopic labeling $C^{13}=O^{18}$ (R_{ISO}) are shown. R_{AI} is the dichroic ratio from the formation of α-helix. β° represents an average tilt angle of α-helical peptides in DMPC, DDPC and DMPG at a peptide-to-lipid ratio of 1:30. Exchanged (%) refers to the percent part of the peptides that are not protected from D_2O exchange, calculated from R_{AI} or R_{AA} (within parentheses). The data is the average of three independent experiments.

Table 4: Toxicity comparison of Cry4Ba and its mutant inclusions against *A. aegypti* larvae

Toxin inclusion	LC_{50} [a]
Cry4Ba-wild type	0.50 (0.36-0.71)
Cry4Ba-R203Q	0.59 (0.37-0.93)

[a] LC_{50} represents toxin inclusion concentration (μg/ml) giving 50% mortality after 24-h exposure to a serial dilution of each toxin inclusion. 95% confidence limits are indicated in parentheses.

Table 5: Crystal diffraction statistics of Cry4Ba-R203Q

Wavelength (Å)	1.00 Å
Temperature (K)	110
Resolution Range (Å)	30.0 – 2.07
Space group	*R*32
Unit-cell parameters (Å)	$a = b$ =184.62, c = 187.36
Unique reflections	74,138 (8,174)[a]
Completeness (%)	99.9 (100)
$< I/\sigma(I) >$	19.8 (4.3)
Average redundancy	6.2
R_{sym} [b] (%)	9.1 (40.4)
Mosaicity (°)	0.25
No. of molecules per asymmetric unit	1
Matthews coefficient ($Å^3$ Da^{-1})	4.33
Solvent content (%)	71.0

[a] Values in parentheses are for the highest resolution shell (2.15-2.07 Å).
[b] $R_{sym} = \sum_{\mathbf{h}} \sum_l |I_{\mathbf{h}l} - \langle I_{\mathbf{h}} \rangle| / \sum_{\mathbf{h}} \sum_l \langle I_{\mathbf{h}} \rangle$, where I_l is the lth observation of reflection $\mathbf{h}$ and $\langle I_{\mathbf{h}} \rangle$ is the weighted average intensity for all observations l of reflection $\mathbf{h}$.

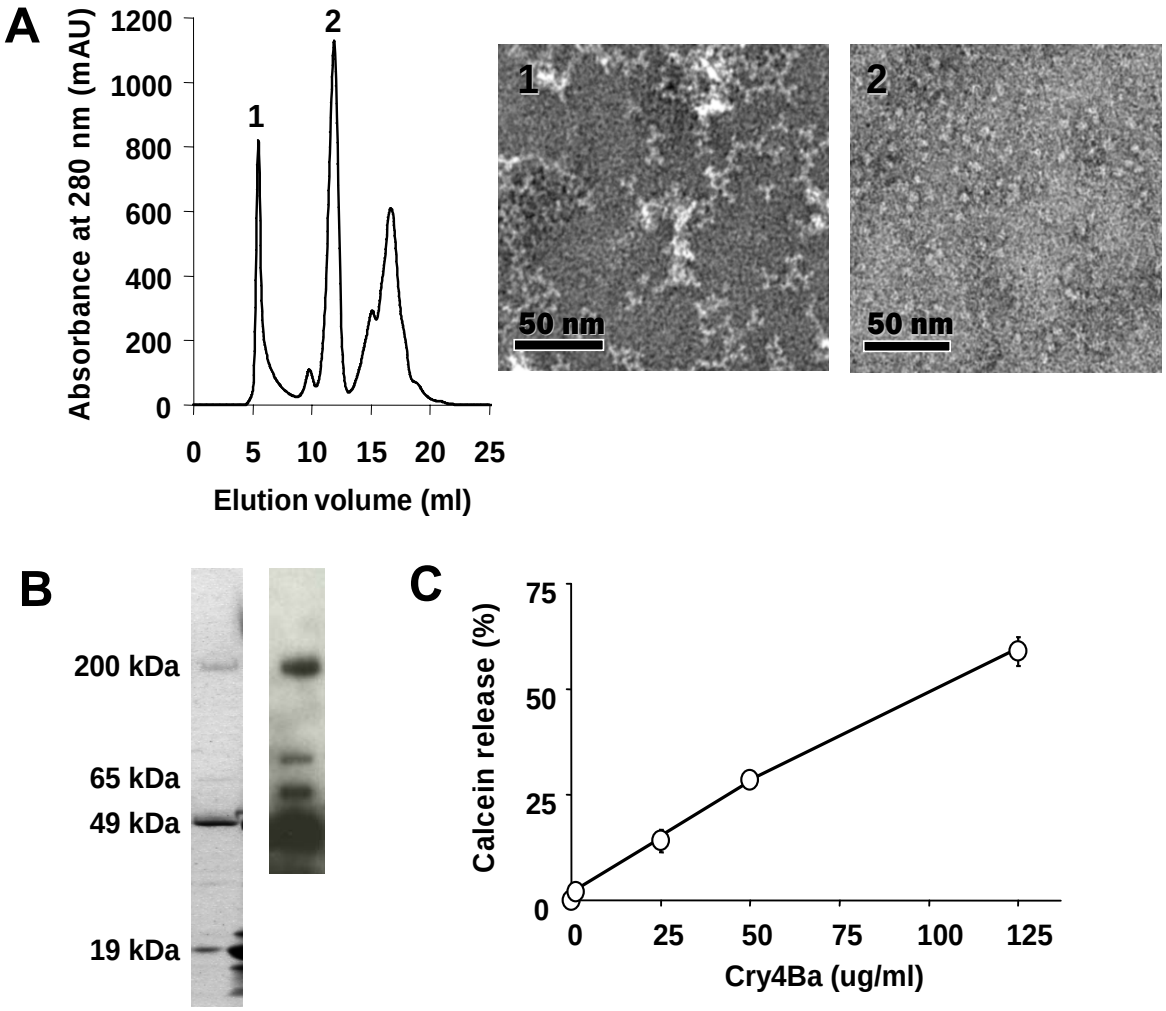

Figure 1: Purification and biochemical characterisation of the 65-kDa activated Cry4Ba toxin. (**A**) Gel filtration analysis of the trypsin-treated Cry4Ba toxin. A Superdex 200 FPLC column was pre-equilibrated with 50 mM Na_2CO_3 buffer, pH 10.5 (**left panel**). The Cry4Ba toxin at approximately 2 mg/ml was applied to the column and eluted with the same buffer. The first protein peak 1 that was eluted with the void volume contained aggregates and apparent oligomers of protein, as can be seen in the first micrograph to the right. Peak 2 contained smaller particles, and eluted at the same time as the 66-kDa BSA protein marker; it was used in subsequent studies. The electron micrographs are of negatively-stained samples of the fractions, stained with 1% uranyl acetate (**right panel**). (**B**) Proteins existed as both monomer (predominantly cleaved into 49- and 19-kDa fragments) and trimer (~200 kDa). Shown are SDS-PAGE analysis of FPLC-purified Cry4Ba toxin (**left lane**) and the corresponding Western blot, probed with the 2F-1H2 monoclonal antibody which is specific to the Cry4Ba domain III fragment. (**C**) Assays for functional pore formation. 10:10:1 (w/w) POPC: POPE: cholesterol liposomes (1 mg/ml) were pre-loaded with calcein (80 mM). Purified toxins were added and the induced release was measured by fluorescence dequenching, with 100% release determined by subsequent addition at a final concentration of 6 mM sodium deoxycholate.

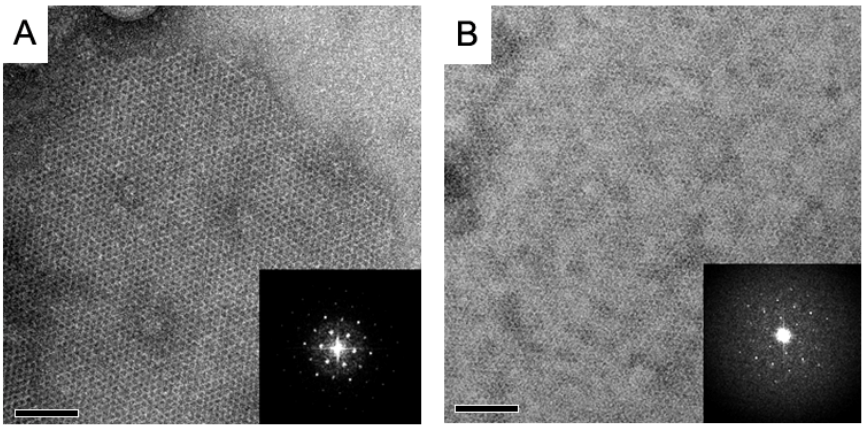

Figure 2: Two types of 2D crystals imaged in negative stain. (**A**) The 65-kDa Cry4Ba toxin crystal grown in DMPC on the air glow discharged carbon surface, and (**B**) the toxin crystal in DMPC attached on the hydrophobic carbon surface. Crystals were up to 1×1 μm in size. Insets show Fourier transforms of these crystalline areas. Insets show Fourier transforms of these crystalline areas. The scale bars are 100 nm.

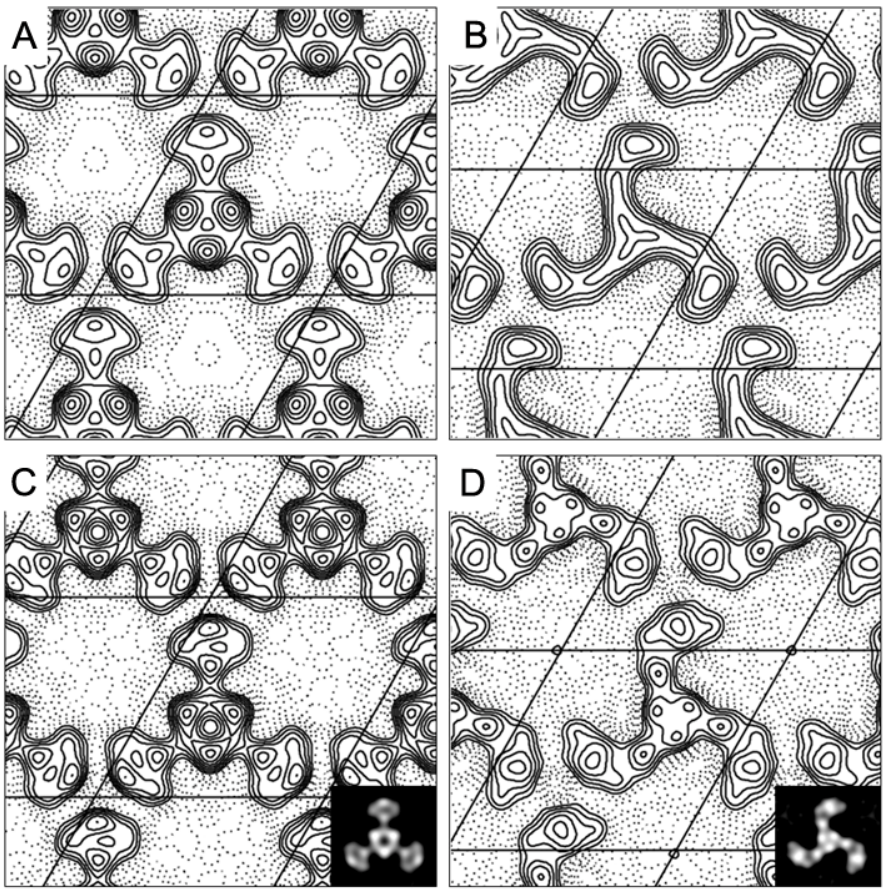

Figure 3: Projection maps of propeller and pinwheel crystal forms. The maps belong to p3 plane group. The contours of the propeller-like and pinwheel-like crystals were plotted at 20 Å (**A**) and (**B**), and at 17 Å resolution (**C**) and (**D**). Insets show reprojection density maps of the propeller-like (**C**) and pinwheel-like structures (**D**).

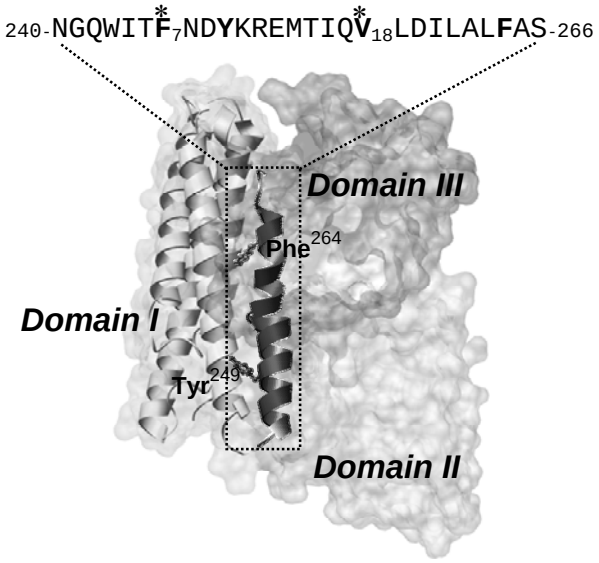

Figure 4: Cry4Ba-helix 7 and its location in the activated toxin structure. Ribbon and surface representation of the Cry4Ba crystal structure with domain I (schematic ribbon) and domains II-III (surface model). Helix 7 (highlighted) within domain I shows the locations of the two critical aromatic residues, Tyr^{249} and Phe^{264} (ball and stick model). Sequence of the synthetic peptide corresponding $\alpha 7$ is illustrated above the structure. Nitrile-derivatised (C≡N) side-chain at Phe^{7} and isotopic labeling at with $C^{13}{=}O^{18}$ Val^{18} (corresponding to the positions Phe^{246} and Val^{257}, respectively) are indicated by *. The structure was generated by using Chimera program.

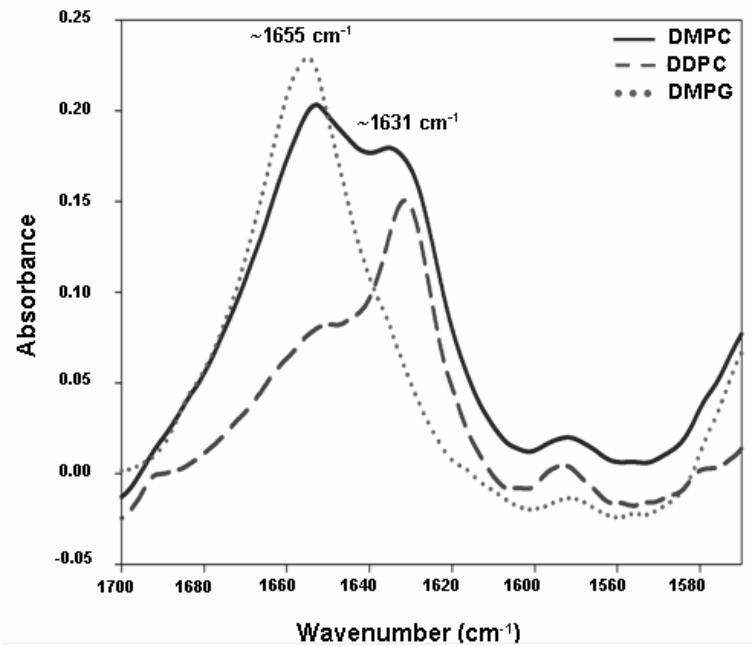

Figure 5: ATR-FTIR spectra of the amide I band for the Cry4Ba-$\alpha 7$ peptide in different phospholipid bilayers. The $\alpha 7$ peptide (labeled with $C^{13}{=}O^{18}$ at Val^{18} and C≡N side-chain at Phe^{7}) was reconstituted in DMPC (——), DMPG (----) and DDPC (….) lipids at a peptide-to-lipid molar ratio of 1:5.

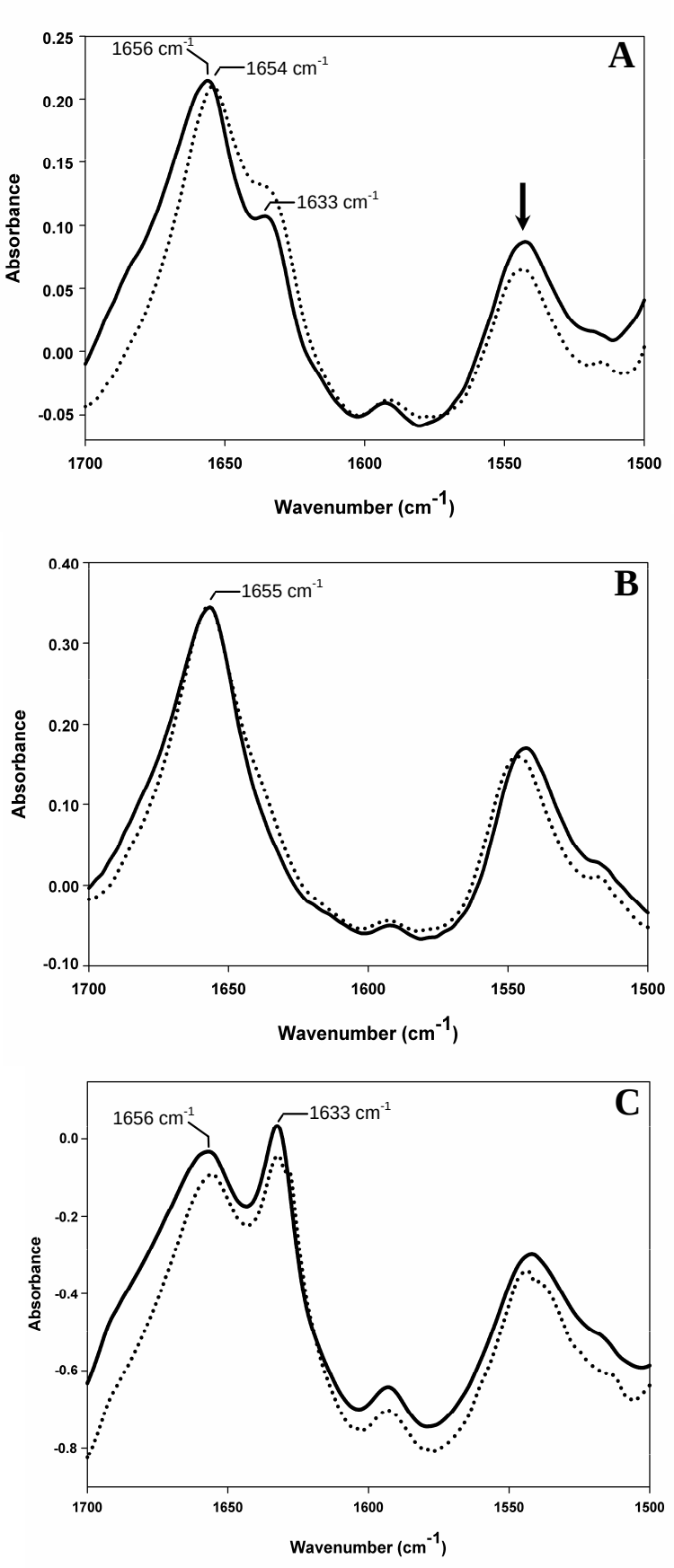

Figure 6: ATR-FTIR spectra of the amide I and II of the Cry4Ba-α7 peptide in H^+/D^+ exchange experiments. The spectra corresponding to the amide I and II before (solid line) and after (dotted line) hydration with D_2O of the Cry4Ba-α7 peptide in DMPC (**A**), DMPG (**B**) and DDPC (**C**) membranes at a peptide-to-lipid molar ratio of 1:30. The peptide used was labeled with $C^{13}=O^{18}$ at Val^{18} and C≡N side-chain at Phe^{7}. The reduction in amide II intensity due to H^+/D^+ exchange is indicated by an arrow.

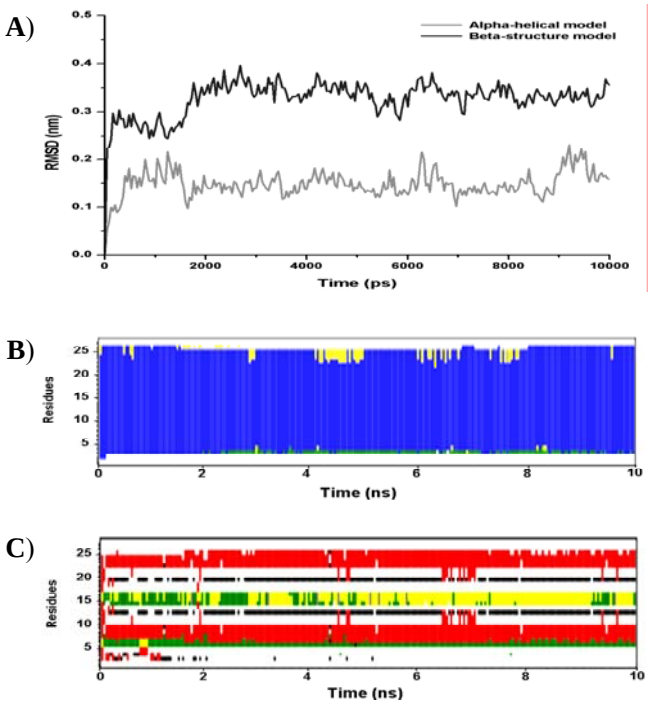

Figure 7: MD simulation trajectories of the Cry4Ba-α7 peptide in DMPC bilayers. **(A)** The root mean square deviation (RMSD) versus time for the C_α atoms in α-helical model or β-structure model. Secondary structures of the Cry4Ba-α7 peptide, analysed using DSSP as a function of simulation time for the α-helical form located at the membrane water-interface region (**B**) and the β-form inserted transversely into the DMPC bilayers (**C**). Grayscale: blue, α-helix; yellow, turn; red, β-sheet; green, bending; black, β-bridge.

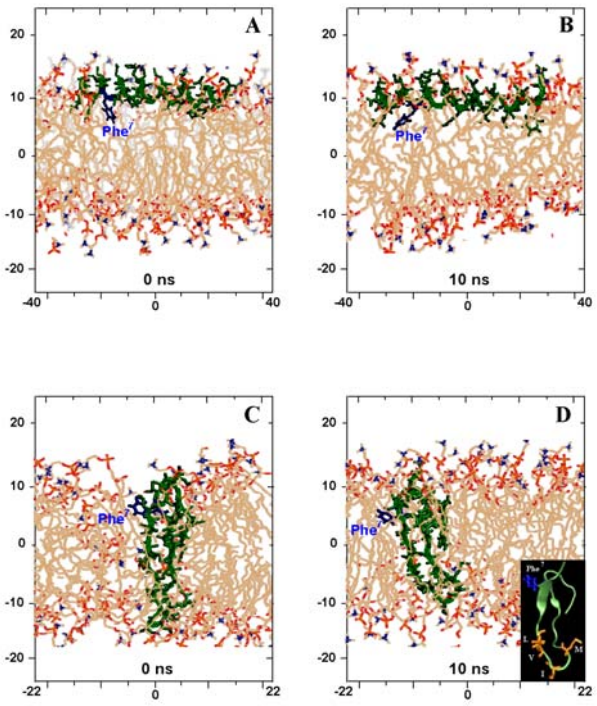

Figure 8: MD snapshots of two conformations of the Cry4Ba-α7 peptide in DMPC bilayers. Snapshots of the MD trajectories of the Cry4Ba-α7 peptide in a fully hydrated DMPC system at simulation times 0 and 10 ns for the membrane-associated helical model (**A-B**), and for the membrane-inserted β-hairpin model (**C-D**). Phe^7 side-chain is indicated and coloured in blue. Inset of **D** illustrates its ribbon model with the hydrophobic turn, Met^{14}, Ile^{16}, Val^{18} and Leu^{19}.

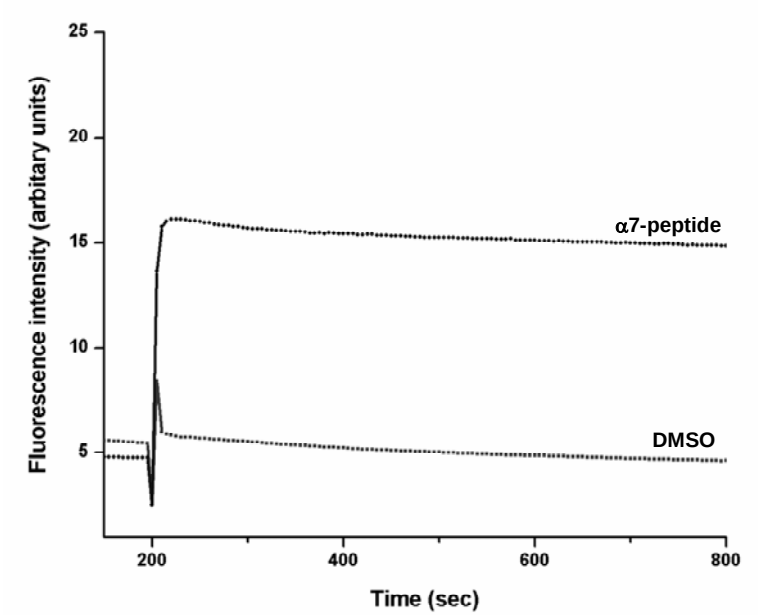

Figure 9: Effects the Cry4Ba-α7 peptide on calcein release from LUVs. The fluorescence intensity of the entrapped calcein upon release from LUVs, which were continuously monitored as a function of time after incubation with the Cry4Ba-α7 peptide at a peptide-to-lipid molar ratio of 1:20 (□). 4 μl of DMSO was used as a negative control (●).

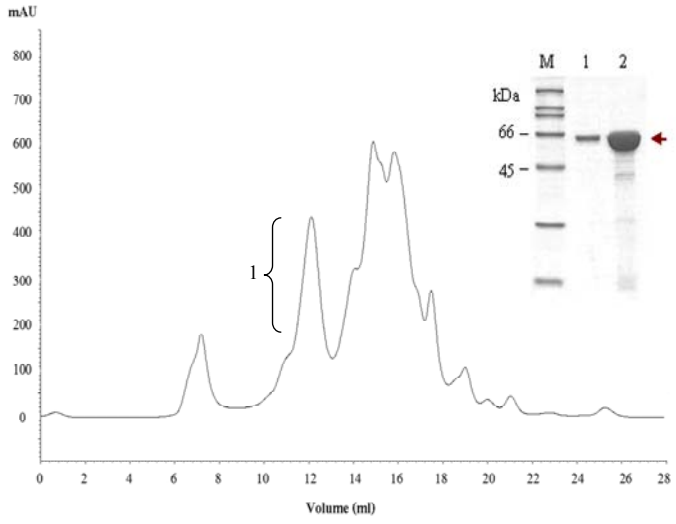

Figure 10: Protein purification of the 65-kDa trypsin-activated Cry4Ba-R203Q mutant by Superdex200 size-exclusion chromatography showing absorbance at 280 nm (mAU) and elution volume (ml). The inset shows SDS-PAGE analysis of the pooled (lane 1) and concentrated (10 mg/ml, lane 2) fractions of peak 1 containing the 65-kDa mutant protein. M represents molecular mass standards.

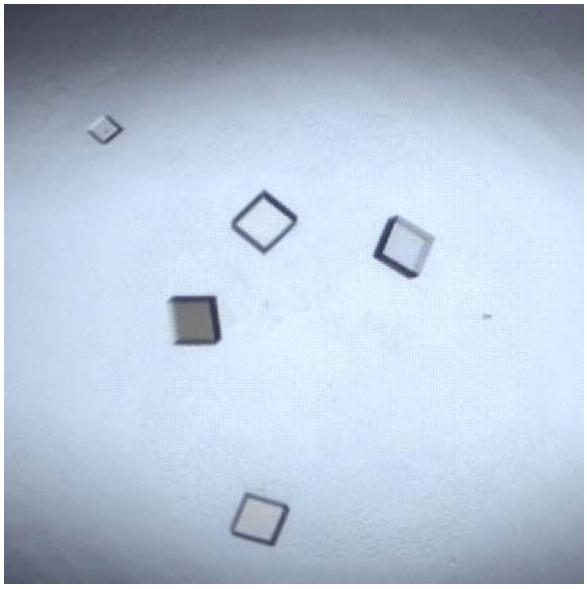

Figure 11: Crystals of the 65-kDa trypsin-activated Cry4Ba-R203Q protein. Approximate dimensions for the largest crystal were 0.07 × 0.07 × 0.02 mm.

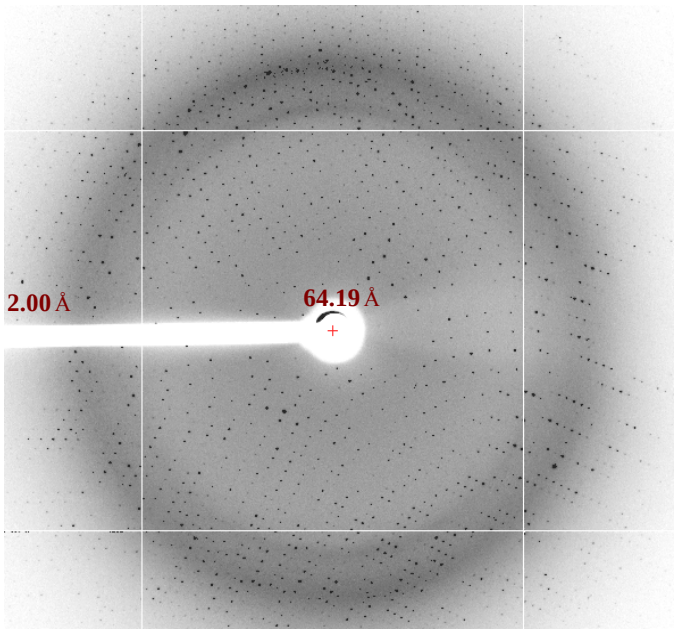

Figure 12: X-ray diffraction pattern through 2.0 Å of a single crystal of the 65-kDa trypsin-activated Cry4Ba-R203Q toxin. The intensity of each diffraction maximum (the darkness of each spot) is a function of the Cry4Ba-R203Q crystal's electron density.

References

Angsuthanasombat, C., Chungjatupornchai, W., Kertbundit, S., Luxananil, P., Settasatian, C., Wilairat, P. and Panyim, S. (1987) Cloning and expression of 130-kd mosquito-larvicidal delta-endotoxin gene of *Bacillus thuringiensis* var. *israelensis* in *Escherichia coli*. *Mol. Gen. Genet.* **208**, 384-389.

Angsuthanasombat, C., Crickmore, N. and Ellar, D.J. (1991) Cytotoxicity of a cloned *Bacillus thuringiensis* subsp. *israelensis* CryIVB toxin to an *Aedes aegypti* cell line. *FEMS Microbiol. Lett.* **83**, 273-276.

Angsuthanasombat, C., Uawithya, P., Leetachewa, S., Pornwiroon, W., Ounjai, P., Kerdcharoen, T., Katzenmeier, G. and Panyim, S. (2004) *Bacillus thuringiensis* Cry4A and Cry4B mosquito-larvicidal proteins: homology-based 3D model and implications for toxin activity. *J. Biochem. Mol. Biol.* **37**, 304-313.

Arkin, I.T., Russ, W. P., Lebendiker, M. and Schuldiner, S. (1996) Determining the secondary structure and orientation of EmrE, a multi-drug transporter, indicates a transmembrane four helix bundle. *Biochemistry* **35**, 7233-7238.

Aronson, A.I., Geng, C. and Wu, L. (1999) Aggregation of *Bacillus thuringiensis* Cry1A toxins upon binding to target insect larval midgut vesicles. *Appl. Environ. Microbiol.* **65**, 2503-2507.

Berendsen, H.J.C., Postma, J.P.M., Gunsteren, W.F.V., Dinola, A. and Haak, J.R. (1984) Molecular dynamics with coupling to an external bath. *J. Chem. Phys.* **81**, 3684-3690.

Boonserm, P., Davis, P., Ellar, D.J. and Li, J. (2005) Crystal structure of the mosquito larvicidal toxin Cry4Ba and its biological implications. *J. Mol. Biol.* **348**, 363-382.

Boonserm, P., Min, M., Angsuthanasombat, C. and Lescar, J. (2006) Structure of the functional form of the mosquito—larvicidal Cry4Aa toxin from *Bacillus thuringiensis* at a 2.8—angstorm resolution. *J. Bacteriol*. **188**, 3391-3401.

Brünger, A.T. (1992) X-PLOR Version 3.1: a system for X-ray crystallography and NMR. Yale University Press, New Haven.

Chia, C.S.B., Torres, J., Cooper, M.A., Arkin, I.T. and Bowie, J.H. (2002) The orientation of the antibiotic peptide maculatin 1.1 in DMPG and DMPC lipid bilayers. Support for a pore-forming mechanism. *FEBS Lett.* **512**, 47-51.

Chou, P.Y. and Fasman, G.D. (1978) Prediction of the secondary structure of proteins from their amino acid sequence. *Adv. Enzymol. Relat. Areas Mol. Biol.* **47**, 45-148.

Crowther, R.A., Henderson, R. and Smith, J.M. (1996) MRC image processing programs. *J. Struct. Biol*. **116**, 9-16.

Crickmore, N. *et al.* Revision of the nomemclature for the *Bacillus thuringiensis* pesticidal crystal proteins. *Microbiol. Mol. Biol. Rev.* **62**, 807-813 (1998).

De Maagd, R.A., Bravo, A. and Crickmore, N. How *Bacillus thuringiensis* has evolved specific toxins to colonize the insect world. *Trends Genet*. **17**, 193-199 (2003).

Derbyshire, D.J., Ellar, D.J. and Li, J. (2001) Crystallization of the *Bacillus thuringiensis* toxin Cry1Ac and its complex with receptor ligand N–acetyl–D–galactosamine. *Acta Crystallogr. Sect. D.* **57**, 1938-1944.

De Maagd, R.A., Weemen—Hendriks, M., Stiekema, W. & Bosch, D. *Bacillus thuringiensis* delta—endotoxin Cry1C domain III can function as a specificity determinant for *Spodoptera exigua* in different, but not all, Cry1—Cry1C hybrids. *Appl. Environ. Microbiol*. **66**, 1559-1563 (2000).

Essmann, U., Perera, L., Berkowitz, M.L., Darden, T., Lee, H. and Pedersen, L.G. (1995) A smooth particle mesh Ewald method. *J. Chem. Phys.* **103**, 8577-8593.

Fernandez, L. E., Martinez-Anaya, C., Lira, E. *et al.* (2009) Cloning and epitope mapping of in the Cry11Aa-receptor Cry11Aa-binding sites alkaline phosphatase from *Aedes aegypti*. *Biochemistry* **48**, 8899-8907.

Gazit, E., la Rocca, P., Samson, M.S. and Shai, Y. (1998) The structure and organization within the membrane of the helices composing the pore-forming domain of *Bacillus thuringiensis* delta-endotoxin are consistent with an "umbrella-like" structure of the pore. *Proc. Natl. Acad. Sci. USA.* **95**, 12289-12294.

Gerber, D. and Shai, Y. Insertion and organization within membranes of the δ–endotoxin pore–forming domain, helix 4–loop–helix 5, and inhibition of its activity by a mutant helix 4 peptide. *J. Biol. Chem.* **275**, 23602-2360726 (2000).

Gómez, I., Sánchez, J., Miranda, R., Bravo, A. and Soberón, M. (2002) Cadherin-like receptor binding facilitates proteolytic cleavage of helix alpha-1 in domain I and oligomer pre-pore formation of *Bacillus thuringiensis* Cry1Ab toxin. *FEBS Lett.* **513**, 242-246.

Grochulski, P. *et al. Bacillus thuringiensis* Cry1A(a) insecticidal toxin crystal structure and channel formation. *J. Mol. Biol.* **254**, 447-464 (1995).

Harrick, N. (1967) Internal reflection spectroscopy. Interscience Publishers, New York.

Hess, B., Bekker, H., Berendsen, H.J.C. and Fraaije, J. (1997) LINCS: a linear constraint solver for molecular simulations. *J. Comput. Chem.* **18**, 1463-1472.

Iacovache, I., Paumard, P., Scheib, H., Lesieur, C., Sakai, N., Matile, S., Parker, M W. and van der Goot, F.G. (2006) A rivet model for channel formation by aerolysin-like pore forming toxins. *EMBO J.* **25**, 457-466.

Jiang, Y., Lee, A., Chen, J., Cadene, M., Chait, B.T. and MacKinnon, R. (2002) Crystal structure and mechanism of a calcium-gated potassium channel. *Nature* **417**, 515-22.

Kumar, A.S. and Aronson, A.I. (1999) Analysis of mutations in the pore-forming region essential for insecticidal activity of a *Bacillus thuringiensis* delta-endotoxin. *J. Bacteriol.* **181**, 6103-6107.

Leetachewa, S., Katzenmeier, G. and Angsuthanasombat, C. (2006) Novel preparation and characterisation of the α4-loop-α5 membrane perturbing peptide from the *Bacillus thuringiensis* Cry4Ba toxin. *J. Biochem. Mol. Biol.* **39**, 270-277.

Li, J., Carroll, J. and Ellar, D.J. Crystal structure of insecticidal δ–endotoxin from *Bacillus thuringiensis* at 2.5 Å resolution. *Nature* **353**, 815-821(1991).

Likitvivatanavong, S., Katzenmeier, G. and Angsuthanasombat, C. (2006) Asn183 in alpha 5 is essential for oligomerisation and toxicity of the *Bacillus thuringiensis* Cry4Ba toxin. *Arch. Biochem. Biophys.* **445**, 46-55.

Loseva, O.I. *et al.* Structure of Cry3A delta-endotoxin within phospholipid membranes. *Biochemistry* **40**, 14143-14151 (2001).

Marsh, D. (1999) Quantitation of secondary structure in ATR infrared spectroscopy. *Biophys. J.* **77**, 2630-2637.

Masson, L., Mazza, A., Sangadala, S., Adang, M.J. and Brousseau, R. (2002) Polydispersity of *Bacillus thuringiensis* Cry1 toxins in solution and its effect on receptor binding kinetics, *Biochim. Biophys. Acta* **1594**, 266-275.

Morse, R.J., Yamamoto, T. & Stroud, R.M. Structure of Cry2Aa suggests an unexpected receptor binding epitope, *Structure* (Camb) **9**, 409-417 (2001).

Muñóz-Garay, C., Portugal, L., Pardo-López, L., *et al*. (2009) Characterization of the mechanism of action of the genetically modified Cry1AbMod toxin that is active against Cry1Ab-resistant insects. *Biochim. Biophys. Acta* **1788**, 2229-2237.

Nunez–Valdez, M. *et al.* Structural and funcional studies of alpha–helix 5 region from *Bacillus thuringiensis* Cry1Ab delta–endotoxin. *Biochim. Biophys. Acta*. **1546**, 122-131 (2001).

Otwinowski, Z. & Minor, W. (1997) Processing of X-ray Diffraction Data Collected in Os. *Methods Enzymol.* **276**, 307–326.

Peyronnet, O., Nieman, B., Genereux, F., Vachon, V., Laprade, R. and Schwartz, J.L. (2002) Estimation of the radius of the pores formed by the *Bacillus thuringiensis* Cry1C delta-endotoxin in planar lipid bilayers. *Biochim. Biophys. Acta* **1567**, 113-122.

Pigott, C.R. and Ellar, D.J. Role of receptors in *Bacillus thuringiensis* crystal toxin activity. *Microbiol. Mol. Biol. Rev.* **71**, 255-281 (2007).

Puntheeranurak, T., Stroh, C., Zhu, R., Angsuthanasombat, C. and Hinterdorfer, P. (2005) Structure and distribution of the *Bacillus thuringiensis* Cry4Ba toxin in lipid membranes. *Ultramicroscopy* **105**, 115-124.

Puntheeranurak, T., Uawithya, P., Potvin, L., Angsuthanasombat, C. and Schwartz, J.L. (2004) Ion channels formed in planar lipid bilayers by the diptheran-specific Cry4Ba *Bacillus thuringiensis* and its α1- α5 fragment. *Mol. Membr. Biol.* **21**, 67-74.

Schnepf, E., Crickmore, N., Van Rie, J., Lereclus, D., Baum, J., Feitelson, J., Zeigler, D.R. and Dean, D.H. (1998) *Bacillus thuringiensis* and its pesticidal crystal proteins. *Microbiol. Mol. Biol. Rev.* **62**, 775-806.

Sigworth, F.J. (1994) Voltage gating of ion channels. *Quat. Rev. Biophys.* **27**, 1-40.

Soberón, M., Pérez, R.V., Nunez-Valdez, M.E., Lorence, A., Gómez, I., Sánchez, J. and Bravo, A. (2000) Evidence for intermolecular interaction as a necessary step for pore-formation activity and toxicity of *Bacillus thuringiensis* Cry1Ab toxin. *FEMS Microbiol. Lett.* **191**, 221-225.

Sramala, I., Uawithya, P., Chanama, U., Leetachewa, S., Krittanai, C., Katzenmeier, G., Panyim, S. and Angsuthanasombat, C. (2000) Single proline substitutions of selected helices of the *Bacillus thuringiensis* Cry4B toxin affect inclusion solubility and larvicidal activity. *J. Biochem. Mol. Biol. Biophys.* **4**, 187-193.

Tamm, L.K. and Tatulian, S.A. (1997) Infrared spectroscopy of proteins and peptides in lipid bilayers. *Quart. Rev. Biophys.* **30**, 365-429.

Tiewsiri, K. and Angsuthanasombat, C. (2007) Structurally conserved aromaticity of Tyr^{249} and Phe^{264} in helix 7 is important for toxicity of the *Bacillus thuringiensis* Cry4Ba toxin. *J. Biochem. Mol. Biol.* **40**, 163-171.

Tigue, N.J., Jacoby, J. and Ellar, D.J. (2001) The alpha-helix 4 residue, Asn135, is involved in the oligomerization of Cry1Ac1 and Cry1Ab5 *Bacillus thuringiensis* toxins. *Appl. Environ. Microbiol.* **67**, 5715-5720.

Tilley, S.J., Orlova, E.V., Gilbert, R.J.C., Andrew, P.W. and Saibil, H.R. (2005) Structural basis of pore formation by the bacterial toxin pneumolysin. *Cell* **121**, 247-256.

Tomimoto, K., Hayakawa, T. & Hori, H. Pronase digestion of brush border membrane–bound Cry1Aa shows that almost the whole activated Cry1Aa molecule penetrates into the membrane. *Comp. Biochem. Physiol. B* **144**, 413-422 (2006).

Unger, V.M., Kumar, N.M., Gilula, N.B. and Yeager, M. (1997) Projection structure of a gap junction membrane channel at 7 Å resolution. *Nature Struct. Biol.* **4**, 39-43.

Vie, V., Van Mau, N., Pomarede, P., Dance, C., Schwartz, J.L., Laprade, R., Frutos, R., Rang, C., Masson, L., Heitz, F. and Le Grimellec, C. (2001) Lipid-induced pore formation of the *Bacillus thuringiensis* Cry1Aa insecticidal toxin. *J. Membr. Biol.* **180**, 195-203.

Vriend, G. (1990) WHAT IF: a molecular modeling and drug design program. *J. Mol. Graph.* **8**, 52-56.

Walters, F.S., Slatin, S.L., Kulesza, C.A. and English, L.H.. Ion channel activity of N–terminal fragments from CryIA(c) delta–endotoxin. *Biochem. Biophys. Res. Commun.* **196**, 921-926 (1993).

Outputs

1. Publications

1.1 Ounjai, P., Unger, V.M., Sigworth, F.J. & **Angsuthanasombat, C.** (**2007**) Two conformational states of the membrane associated *Bacillus thuringiensis* Cry4Ba δ-endotoxin complex revealed by electron crystallography: Implications for toxin-pore formation. ***Biochem. Biophys***. ***Res. Commun.*** 361: 890-895.

1.2 Tiewsiri, K., Fischer, W. & **Angsuthanasombat, C.** (**2009**) Lipid-induced conformation of helix 7 from the pore-forming domain of the *Bacillus thuringiensis* Cry4Ba toxin: Implications for toxicity mechanism ***Arch. Biochem. Biophys***. 482: 17-24.

1.3 **Angsuthanasombat, C.** (**2010**) Structural basis of pore formation by mosquito-larvicidal proteins from *Bacillus thuringiensis*. ***Open Toxinol. J.*** (In press).

1.4 Thamwiriyasati, N., Sakdee, S., Chuankhayan, P., Katzenmeier, G., Chen, C-J & **Angsuthanasombat, C.** (**2010**) Crystallization and preliminary X-ray crystallographic analysis of a full-length active form of Cry4Ba toxin from *Bacillus thuringiensis*. ***Acta Cryst. F*** (In press)

1.5 Taveecharoenkool, T., **Angsuthanasombat, C.** & Kanchanawarin, C. (**2010**) Combined molecular mechanics and continuum solvent studies suggest that the pre-pore trimer of Cry4Aa toxin from *Bacillus thuringiensis* is stable in solution. ***PMC Biophys.*** (In press)

2. Graduates

Ph.D. in ***Molecular Genetics and Genetic Engineering***

Mr. Puey Ounjai
Date of Graduation: 24 August 2007
Thesis Title:
"Molecular Biophysical Study of the *Bacillus thuringiensis* Cry4Ba Toxin Pore Structure"

Miss Niramon Thamwiriyasati
Date of Graduation: 25 March 2010
Thesis Title:
"Structural and Functional Characterization of the *Bordetella pertussis* CyaC Acyltransferase"

Ph.D. in ***Immunology***

Mr. Taweechai Taweecharuenkul
Date of Graduation: 29 April 2008
Thesis Title:
"Molecular Dynamics Simulations of the *Bacillus thuringiensis* Cry4Aa and Cry4Ba Toxin"